Decoding Single-Hand and Both-Hand Movement Directions from Noninvasive Neural Signals

Jiarong Wang, Luzheng Bi*, *Senior Member, IEEE*, Weijie Fei, and Cuntai Guan, *Fellow, IEEE*

Abstract—Decoding human movement parameters from electroencephalograms (EEG) signals is of great value for human-machine collaboration. However, existing studies on hand movement direction decoding concentrate on the decoding of a single-hand movement direction from EEG signals given the opposite hand is maintained still. In practice, the cooperative movement of both hands is common. In this paper, we investigated the neural signatures and decoding of single-hand and both-hand movement directions from EEG signals. The potentials of EEG signals and power sums in the low frequency band of EEG signals from 24 channels were used as decoding features. The linear discriminant analysis (LDA) and support vector machine (SVM) classifiers were used for decoding. Experimental results showed a significant difference in the negative offset maximums of movement-related cortical potentials (MRCPs) at electrode Cz between single-hand and both-hand movements. The recognition accuracies for six-class classification, including two single-hand and four both-hand movement directions, reached 70.29%± 10.85% by using EEG potentials as features with the SVM classifier. These findings showed the feasibility of decoding single-hand and both-hand movement directions. This work can lay a foundation for the future development of an active human-machine collaboration system based on EEG signals and open a new research direction in the field of decoding hand movement parameters from EEG signals.

Keywords—Both-hand movement, brain-computer interface, EEG, hand movement decoding, movement-related cortical potential, neural signature

I. INTRODUCTION

HUMAN-MACHINE collaboration has attracted increasing attention in recent years. Human movement parameter (intention) recognition plays a vital role in an active human-machine collaboration, which can help improve the performance of the whole human-machine systems.

There are mainly two kinds of physiological signals used to recognize (or decode) human movement intention: electroencephalograms signals (EEG signals) and electromyography signals (EMG signals) [1] [2]. Compared with using EMG signals, using EEG signals could detect motion intention more quickly [3]. In human-machine collaboration systems, decoding human movement intention earlier can better help users to perform the specified task or warn them [4]. In this paper, we focus on hand movement parameter decoding from EEG signals.

EEG-based movement intention decoding is an essential branch in the area of brain-computer interfaces (BCIs). Over the past decades, there are many studies about the establishment and improvement of BCI systems. For example, in 1988, Farwell *et al.* [5] developed a spelling system to select letters on the screen by using P300. In 1991, Wolpaw *et al.* [6] first studied the EEG-based BCI for cursor control. In 2014, Bi *et al.* [7] proposed a new steady-state visually evoked potential BCI to continuously control a simulated vehicle with a 14-DOF dynamics model. In 2019, Edelman *et al.* [8] used EEG signals to achieve the neural control of a robotic device for continuous target tracking. Compared with motor imagery-based or visual evoked potentials-based BCIs, decoding movement parameters directly from EEG signals can provide an intuitive and natural control [9].

In recent years, a large number of studies have shown that it is feasible to decode hand movement parameters from EEG signals. In 2008, Waldert *et al.* [10] used EEG signals to decode center-out movements with the hand and obtained a binary decoding accuracy of 55% on average across subjects. In 2009, Bradberry *et al.* [11] proposed a decoding model that can extract hand kinematic information from EEG signals and reconstruct the trajectory and velocity of hand with the correlation coefficients of 0.2 and 0.3, respectively. In 2013, Robinson *et al.* [12] proposed a model that used the wavelet-common spatial pattern algorithm to decode hand movement in four orthogonal directions from EEG signals, which yielded an average binary classification accuracy of 80%. In 2015, Jochumsen *et al.* [13] detected and classified movement-related cortical potentials (MRCPs) associated with hand movement in healthy subjects and stroke patients and showed the possibility of using the single EEG channel for detecting hand movement intention. In 2018, Chouhan *et al.* [14] proposed a wavelet phase-locking value-based method for binary classification of hand movement, and the binary classification of movement direction reached the mean accuracy of 76.85%. Considering

L. Bi, J. Wang, and W. Fei are with the School of Mechanical Engineering, Beijing Institute of Technology, Beijing 100081 China. (e-mail: bhxblz@bit.edu.cn, 18810805389@163.com, 3120170241@bit.edu.cn).
C. Guan is with the School of Computer Science and Engineering, Nanyang Technological University. (ctguan@ntu.edu.sg)

that unimanual upper-limb neuroprostheses control for a paraplegic patient is not enough, Schwarz *et al.* [15] investigated how to discriminate unimanual and bimanual reach-and-grasp actions, which are common and important for daily life. Experimental results from able-bodied subjects showed the possibility of discriminating bimanual from unimanual grasp movements, although the average recognition accuracy of the seven-class classification was peaking at 38.6%.

However, to the best of our knowledge, no existing studies on hand movement decoding from EEG signals explore how to decode single-hand and both-hand movement parameters (including direction, acceleration, velocity, and trajectory). In practice, to use a device to complete a specific task, sometimes, able-bodied operators need to use a single hand to operate a human-machine interface (such as a joystick), while keeping the second hand still. Sometimes, they need to use both hands to operate two human-machine interfaces (such as two joysticks), respectively, and two hands often need to execute movements in different directions. Thus, for developing active human-centric assistive systems to better assist operators in performing tasks, decoding single-hand and both-hands movement parameters is worth being explored.

In this paper, we investigate how to discriminate the neural signatures of both-hand movement directions from those of single-hand movement directions and how to decode single-hand and both-hand movement directions. The contribution of this paper is that it is the first work to investigate the neural signatures and decoding of single-hand and both-hand movement directions. This work can lay a foundation for the future development of an active human-machine collaboration system based on EEG signals and open a new research direction in decoding hand movement parameters from EEG signals.

The remainder of the paper is organized as follows: Section II introduces the method. Section III presents the results. Section IV describes the discussion, limitations of our work, and future work. Section V describes the conclusion.

II. METHOD

A. Experimental Paradigm and Procedure

Eight healthy subjects (aged 22-25 years, one female) participated in the experiment. All of them were right-handed and had normal vision. Every subject was confirmed to have no brain diseases. The study adhered to the principles of the 2013 Declaration of Helsinki.

Since all subjects are right-handed in our experiment, we regarded the right-hand movement as the single-hand movement to be decoded and the left-hand movement as the secondary movement. We required all subjects to move their right hands in horizontal directions (*right* or *left*). Considering that two hands often move in different directions in practical human-machine collaboration systems, we preliminarily set the left-hand movement in vertical directions (*up* or *down*) rather than horizontal directions. Both hands were moved in the 2-D horizontal plane. Figs. 1 and 2 show the experimental setup and protocol, respectively. There were six sessions in all. Two of them were right-hand movements in the *right* and *left* directions without the left-hand movement, respectively. The remaining four sessions were the right-hand movements in the *right* and *left* directions with the left-hand movement in the *up* and *down*

Fig.1. Experimental setup.

directions, respectively. Each experimental session was composed of five runs, with a rest period of 2 minutes in between. Each run consisted of 16 trials.

When one trial started, two target positions (red and green solid blocks correspond to the target positions of the left and right hands, respectively) appeared in specified directions, and the subjects were required to prepare for the movement during this period. At the fourth second of the experiment, the computer indicated subjects to execute the movement by changing two target positions on the screen from the solid to hollow blocks, and the subjects started to use left and right hands to move the corresponding blocks from the center to target positions. At the seventh second, both blocks were asked to be in the target positions, and then the subjects were acquired to move both hands back to the center position. Before the actual movement execution, the subjects were required to keep their eyes fixed on the green block (corresponding to the right hand) to reduce the interference of eye movements. Subjects were instructed not to make any body movements unrelated to the experimental requirements.

B. Data Acquisition

The experiment was performed at the IHMS Lab of the School of Mechanical Engineering, Beijing Institute of Technology, China. EEG signals were acquired by a 64-electrode portable wireless EEG amplifier (NeuSen.W64, Neuracle, China) from the scalp of subjects at the Fz, F3, F4, Cz, C1, C2, C3, C4, FCz, FC3, FC4, Pz, P3, P4, P7, P8, T7, T8, Oz, O1, O1, POz, CP3, CP4 locations according to an international 10-20 system, with a forehead ground at AFz and reference placed at CPz. Electrooculogram (EOG) signals were acquired from two electrodes positioned below the outer canthi of the eyes. The sampling rate was set to be 1000 Hz. Electrode impedances were calibrated to be less than 5 KΩ. We collected the positions of both hands by using the motion position tracking equipment *FASTRACK* at a sampling rate of 60 Hz.

C. Data Analysis

EEG signals were down-sampled to 100 Hz. The EEG signals from each channel were re-referenced by binaural electrodes. We defined the time when the subjects were indicated to execute the motion as the movement cue onset, i.e., the fourth second in the experiment. The actual movement onset was calibrated by *FASTRACK* and was 0.5 s after the movement cue onset. Trials were rejected according to the two criteria: (1) amplitude threshold exceeding ±300 μV and (2) trials with abnormal kurtosis. Furthermore, the standard independent component analysis for EOG removal by using
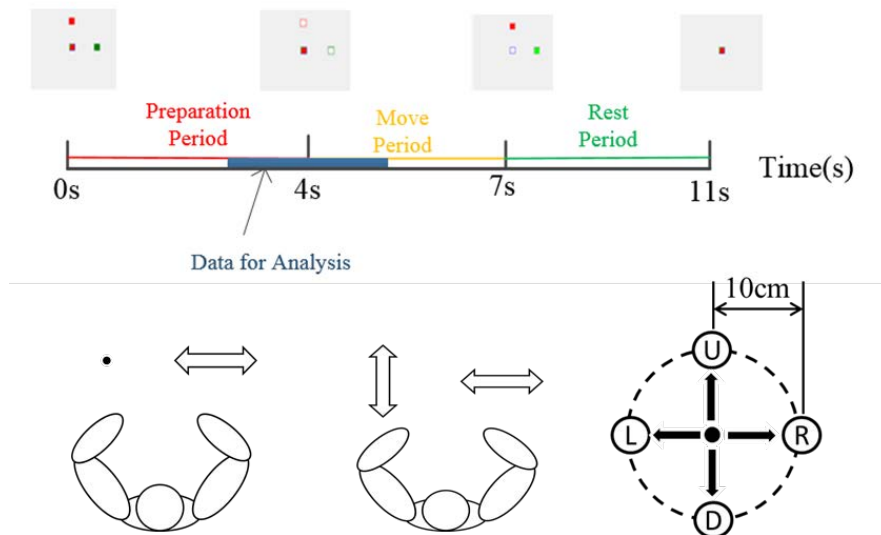
Fig. 2. Experimental paradigm

EEGLab was applied. For the muscle artifacts, we did not take a further preprocessing since muscle artifacts are in the high-frequency band (generally higher than 20 Hz) instead of the low-frequency band (e.g., less than 6 Hz) used in our study, and the work [16] shows that muscle artifacts do not provide any discriminative information about the decoding performance. All data processing was done in MATLAB.

1) Movement Related Cortical Potential (MRCP): MRCP is a spontaneous potential that is generated by the execution or imagination of movement. Studies show that MRCPs encode movement information [9] [15]. Thus, MRCPs were extracted to present neural signatures of brain activity during the experimental period [17]. For the MRCP detection, the filtering is critical since the low signal-to-noise ratio of EEG signals [18]. We first applied a baseline correction to suppress the zero drift of signals. To remove the global background activity, we used a common average referencing (CAR). After that, a fourth-order [0.01-4] Hz band-pass Butterworth filter was used to reserve the low-frequency component of EEG signals. The weighted average (WAVG) filter was applied to the Cz channel to improve the performance of the MRCP detection. The WAVG was calculated by $e_i(t) = e_i(t) + 1/K \sum_{j=1}^{K} e_j(t)$, where $e_i(t)$ is the EEG signal of the ith channel and K is the number of the nearest neighbor channels (Because CPz was selected as the reference electrode in our experiment, the residual three orthotropic nearest channels were selected, i.e., K=3) [19]. The epoch [-1.5, 1.5] s of the movement cue onset during each trial was selected for analysis. For each experimental session, 80 samples were extracted. Totally, for the sessions of single-hand movement, there were 80*2 samples, and for the sessions of both-hand movement, there were 80*4 samples.

2) Feature Extraction and Decoding: Baseline correction was first used to eliminate the drift. To suppress the effect of movement artifacts on decoding performance, we applied artifact subspace reconstruction (ASR) [20]. ASR could automatically identify and utilize the clean potions of EEG

signals as the reference data, and subsequently determine the rejection thresholds to reject artifact components and reconstruct cleaned data. The cut-off parameter k, which was used to define rejection thresholds, was empirically defined as 10 in this study, and ASR was performed using the open-source plug-in function clean_asr in EEGLab [20]. CAR and a fourth-order [0.01-4] Hz band-pass Butterworth filter were then applied. After signal preprocessing, we obtained the preprocessed signals for classification. For each window of 1 s, we adopted the potential amplitude of EEG signals from each channel at each sampling point as a feature. That is, there were 100 features for each channel. All potential amplitudes of 24 channels were concatenated into a 2400-dimension feature vector, which is defined as Temporal feature. Furthermore, we calculated the power sum of the frequency band [0.01, 4] Hz of EEG signals from each channel as a classification feature. The power sums of 24 channels were concatenated into a 24-dimension feature vector, which is defined as Spectral feature [21].

To address feature redundancy and reduce computational time, we applied principal component analysis (PCA) to the original features [22]. For the Temporal feature, the dimension of the feature was reduced from 2400 to 40 by using the PCA. For the Spectral feature, the feature dimension was 24, and no PCA was performed.

To address the multi-classification of different movement conditions (6 conditions: namely *right*, *left*, *right-up*, *right-down*, *left-up*, and *left-down* in short), we adopted a one-versus-one classification strategy. For six kinds of movement conditions, 15 binary classification models were yielded. The predicted labels were decided by majority voting, and if multi-labels are voted equally, the final predicted label is randomly selected. The decoding was performed on a continuous sliding window to observe the decoding performance changing over time, and the length of the window was set to be 1 s, and the step size was set to be 0.1 s. The decoding of the hand movement direction was performed by the LDA and SVM,

respectively [23].

The LDA model is as follows:

$$f(\text{x}) = \omega^{\text{T}}\text{x} + \omega_0, \qquad (1)$$

where $\text{x} = [\text{x}_1, \text{x}_2, \cdots, \text{x}_n]$ is the sample vector, $\omega = [\omega_1, \omega_2, \cdots, \omega_n]$ represents the projecting directions of the classifier, and ω_0 represents the threshold of the classifier, which is determined by receiver operating characteristic curve (ROC). Mean decoding accuracies were calculated by the 10×8 cross-validation method over all subjects.

The SVM classifier is as follows:

$$f(\text{x}) = \text{sgn}(\textstyle\sum_{i=1}^{v} y_i \alpha_i K(x, x_i) + b), \qquad (2)$$

where y_i is the classification label, x_i is the i th support vector, α_i is the Lagrange factor of x_i, v is the number of support vector, and $K \cdot$ is the kernel function. In this study, radius basis function was used as kernel function, which can be written as

$$K(x, x_i) = \exp(-g * \|x - x_i\|^2) \qquad (3)$$

The parameters of kernel function g and the slack variable c are critical for training the SVM model. We randomly divided the whole dataset into the calibration set (75%) and evaluation set (25%). In the calibration set, we utilized the mesh grid method to establish different training models corresponding to different parameters c and g and evaluated the training model performance by six-fold cross validation. The training model with the best decoding performance was selected, and the ultimate model performance was tested on the evaluation set. The above procedure was repeated ten times at random to obtain the average decoding results by using SVM. The SVM algorithm in this study was applied based on LIBSVM 2.0 toolbox supported by Chih-Chung Chang and Chih-Jen Lin *et al* [24].

D. Statistics

We used a two-factor repeated measure analysis of variance (ANOVA) on decoding accuracy. The two factors were classification feature (Temporal feature and Spectral feature) and classifier (LDA classifier and SVM classifier) [25]. The significant level was set to be 0.05.

III. RESULTS

A. Neural Signatures

Fig. 3 shows the average MRCPs associated with six kinds of movement conditions. All average MRCPs were calculated by using EEG signals at electrode Cz from -1.5 s to 1.5 s with respect to the movement cue onset across all subjects. The amplitude of MRCPs was steady during the preparation period, and the negative offset of MRCPs appeared at around 300 ms and reached the maximum amplitude at about 500 ms, and the latter was consistent with the actual movement onset recorded by *FASTRACK*. In addition, the amplitude of the MRCPs in the movement period was larger than that in the non-movement period, which is in accord with the finding in [26].

As shown in Fig. 3, by comparing MRCPs under different movement conditions, we found larger negative offset amplitudes under the conditions of both-hand movement. Furthermore, larger negative offset amplitudes were observed
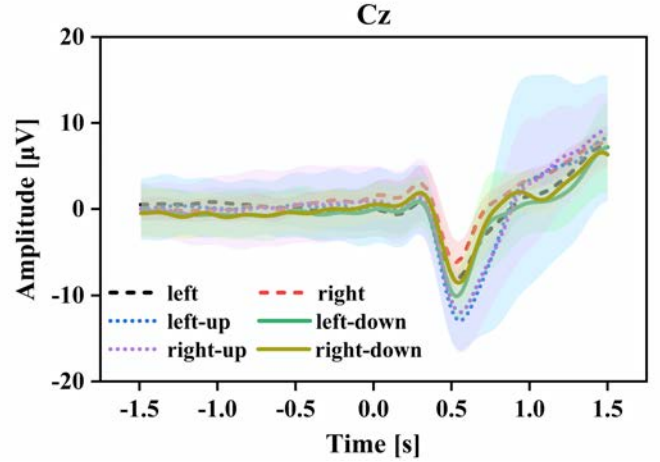
Fig. 3. The averaged MRCPs across all subjects at *Cz* channel from -1.5 s to 1.5 s of motion execution under six types of movement conditions. "Left" and "Right" refer to the right-hand movement in *left* and *right* directions. "Up" and "Down" refer to the left-hand movement in *up* and *down* directions in the 2-D horizontal plane. Note that time 0 s refers to the time point when the movement cue appears, and time 0.5 s is the onset of the actual movement.

under the condition of left-hand movement in *up* direction than in *down* direction. Given the same left-hand movement conditions, larger negative offset amplitudes could also be observed under the condition of right-hand movement in *left* direction than in *right* direction. For the single-hand movement, the average negative offset maximums of the MRCP for right-hand movements in *right* and *left* directions were -6.15 μV and -7.99 μV, respectively. For the left-hand movement in *down* direction, the negative offset maximums of the MRCP for right-hand movements in *right* and *left* directions were -8.52 μV and -10.09 μV, respectively. For the left-hand movement in *up* direction, the negative offset maximums of the MRCP for right-hand movements in *right* and *left* directions were -11.97 μV and -12.90 μV, respectively. MRCPs associated with six kinds of movement conditions at electrode C1 and C2 are showed and described in Supplementary Fig. 1 and Fig. 2, respectively.

Fig. 4 shows the average MRCPs at electrodes C1, Cz, and C2 associated with the single-hand movement and both-hand movement. The MRCPs associated with the single-hand movement were the average results of MRCPs obtained under the right-hand movements in directions *left* and *right*. The MRCPs associated with the both-hand movement were the average results of MRCPs obtained under the left-hand movements in directions *up* and *down* and right-hand movements in directions *left* and *right*. For avoiding the effect of amplitudes at electrode Cz on electrodes C1 and C2, no WAVG filter was performed in this step. As shown in Fig. 4, for the single right-hand movement, larger negative offset amplitude was obtained on contralateral electrode C1 than on ipsilateral electrode C2, although the statistics test was not significant (-3.89 μV VS -2.67 μV, paired t-test, $p = 0.3280$). On electrode C1, similar negative offset amplitudes were
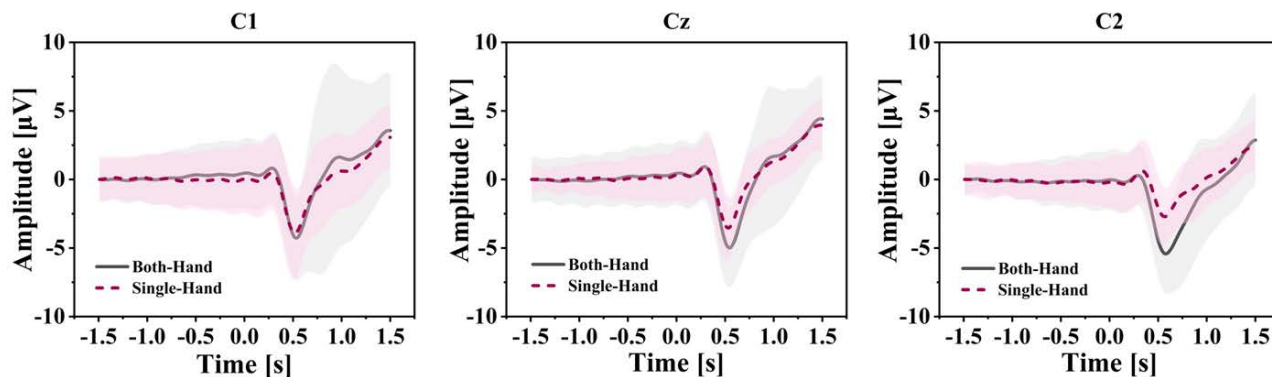
Fig. 4. The averaged MRCPs at Cz, C1 and C2 channel from -1.5 s to 1.5 s of motion preparation and execution under conditions of single-hand movement and both-hand movement. The shadows shown in figures are the standard deviation of MRCPs across all subjects. Note that time 0 s refers to the time point when the movement cue appears, and time 0.5 s is the onset of the actual movement.
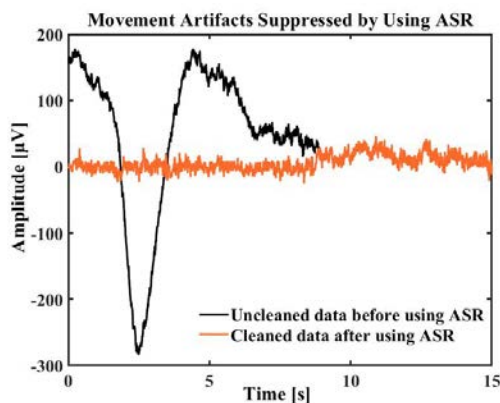
Fig. 5. Comparison of EEG signals contaminated by movement artifacts before and after applying ASR for cleaning and reconstructing data.

Fig. 6. Grand average decoding performance comparison among models built by using Temporal and Spectral features with LDA and SVM classifiers. The continuous 6-class classification was executed on shifted windows from -2 s to 2s of movement cue onset. Note that time 0 s refers to the time point when the movement cue appears, and time 0.5 s is the onset of the actual movement. After 0 s, actual movement information started to be involved in shifted windows.

obtained for the single-hand and both-hand movement (both containing right-hand movement), and were -3.89 µV and -4.27 µV, respectively (paired t-test, $p = 0.1999$). On electrode Cz, a larger negative offset amplitude was obtained for both-hand movement than single-hand movement (-3.54 µV VS -4.99 µV, paired t-test, $p = 0.0481$). On electrode C2, a larger negative offset amplitude was obtained for both-hand movement, which contained left-hand movement than single-hand movement (i.e., single right-hand movement) (-5.41 µV VS -2.67 µV, paired t-test, $p = 0.0300$).

B. Movement Artifacts Suppressed by ASR Cleaning

This study focused on single-hand and both-hand center-out movement, and the removal of movement artifacts is critical. ASR is an automatic method to remove transient or large-magnitude artifacts contaminating EEG data, which are usually caused by movement. Fig. 5 shows a typical example for movement artifacts suppressed by using ASR for cleaning and reconstructing EEG signals. For the raw signals without using ASR, a large-magnitude-and-slow wave was observed. By applying the ASR cleaning, the large-magnitude related components were rejected, and the reconstructed EEG signals showed well modality without evident movement artifacts contamination.

C. Multi-classification Performance

Fig. 6 illustrates the 6-class continuous decoding performance comparison by using two kinds of decoding features and two classifiers. TABLE I shows the confusion matrices of each type of models on the window of [0.5 1.5] s. The average decoding accuracies were calculated across all subjects. The decoding was done on shifted windows with a length of 1 s and a step size of 0.1 s, and the center time point of each window was used to represent this window. During the time period from -2 s to 2 s of the movement cue onset, 31 windows were involved. As shown in Fig. 6, the decoding performance was steady before 0 s, and gradually increased after 0 s. The decoding accuracies of models built by Temporal feature with SVM classifier, Temporal feature with LDA classifier, Spectral feature with SVM classifier, and Spectral

TABLE I. CONFUSION MATRICES OF FOUR TYPES OF MODELS BY USING TEMPORAL AND SPECTRAL FEATURES WITH LDA AND SVM CLASSIFIERS, RESPECTIVELY. THE RESULTS WERE AVERAGED ACROSS ALL SUBJECTS.

LDA Temporal (True rows / Predicted columns)

True \ Predicted	Left	Right	Left-Up	Right-Up	Left-Down	Right-Down
Left	50.38%	15.31%	7.34%	6.31%	11.53%	9.13%
Right	13.34%	60.38%	7.28%	3.72%	7.84%	7.43%
Left-Up	7.15%	7.88%	58.34%	8.94%	9.94%	7.75%
Right-Up	7.81%	4.34%	7.19%	71.66%	3.75%	5.25%
Left-Down	10.72%	6.69%	9.03%	3.47%	60.53%	9.56%
Right-Down	6.88%	7.53%	6.22%	4.72%	8.81%	65.84%

LDA Spectral (True rows / Predicted columns)

True \ Predicted	Left	Right	Left-Up	Right-Up	Left-Down	Right-Down
Left	40.28%	16.00%	9.06%	9.03%	12.97%	12.66%
Right	11.66%	50.44%	3.91%	11.25%	10.38%	12.38%
Left-Up	9.59%	6.16%	50.56%	9.13%	15.72%	8.84%
Right-Up	7.19%	11.22%	8.41%	50.88%	8.19%	14.13%
Left-Down	11.63%	10.25%	13.91%	9.38%	48.16%	6.69%
Right-Down	8.75%	14.34%	5.53%	12.22%	9.03%	50.13%

SVM Temporal (True rows / Predicted columns)

True \ Predicted	Left	Right	Left-Up	Right-Up	Left-Down	Right-Down
Left	64.00%	11.88%	4.63%	5.13%	7.75%	6.63%
Right	12.75%	66.13%	3.88%	3.25%	7.13%	6.88%
Left-Up	9.25%	5.75%	67.88%	4.88%	7.00%	5.25%
Right-Up	6.13%	3.88%	5.75%	76.88%	2.25%	5.13%
Left-Down	11.00%	6.75%	8.25%	3.13%	65.75%	5.13%
Right-Down	7.50%	6.25%	5.63%	5.25%	6.38%	69.00%

SVM Spectral (True rows / Predicted columns)

True \ Predicted	Left	Right	Left-Up	Right-Up	Left-Down	Right-Down
Left	47.5%	15.38%	10.63%	8.75%	10.50%	7.25%
Right	16.25%	51.75%	5.25%	7.50%	9.25%	10.00%
Left-Up	11.00%	5.38%	61.63%	4.63%	10.5%	6.88%
Right-Up	11.38%	13.75%	6.25%	51.63%	5.00%	12.00%
Left-Down	13.88%	14.00%	11.75%	6.13%	46.00%	8.25%
Right-Down	9.25%	11.00%	7.63%	11.00%	7.88%	53.25%

TABLE II. SUBJECT-INDEPENDENT SIX-CLASS CLASSIFICAITON PEAK ACCURACY AND PEAK TIME USING DIFFERENT TYPES OF MODELS.

Subject No.	LDA Classifier				SVM Classifier			
	Peak Accuracy [%]		Peak Time [s]		Peak Accuracy [%]		Peak Time [s]	
	Temporal	Spectral	Temporal	Spectral	Temporal	Spectral	Temporal	Spectral
S1	74.13	56.75	0.5	0.9	81.83	61.67	0.8	0.8
S2	55.00	42.12	1.4	0.9	61.00	48.50	1.2	0.9
S3	70.92	65.88	1.1	1.2	80.50	71.67	1.1	0.9
S4	55.33	47.25	1.0	0.8	62.67	52.00	0.9	0.9
S5	56.46	47.38	0.9	1.5	67.00	52.83	0.9	1.4
S6	71.12	61.37	0.7	1.1	78.17	66.17	1.0	1.2
S7	71.75	50.67	1.8	0.9	78.33	58.67	1.1	0.9
S8	53.71	38.33	0.8	0.9	52.83	36.00	1.0	0.8
Mean± Std	63.55± 9.09	51.22± 9.47	1.03± 0.41	1.03± 0.23	70.29± 10.85	55.94± 11.15	1.00± 0.13	0.98± 0.21

feature with LDA classifier peaked at 0.8 s, 0.9 s, 0.9 s, and 0.9 s, and were 69.02%± 11.45%, 61.91%± 9.48%, 54.72%± 11.04%, and 49.31%± 9.42%, respectively. Furthermore, for the models mentioned above, decoding accuracies on the movement cue onset (0 s) were 46.60%± 10.56%, 39.33%±8.55%, 40.40%±8.03%, and 37.40%± 6.82%, respectively. For the 6-class classification, the chance level was 16.67%, and the decoding performance of both preparation period (-2 s to 0 s) and movement period (0 s to 2 s) was all above chance level. As shown in TABLE I, relatively high true positive rate (TPR) results were obtained except the movement condition of left, under which the decoding accuracy was lower than under other movement conditions by 5% to 20%. Given the low TPR obtained under the movement condition of left, the predicted labels were mainly mistaken for the movement

condition of right. Overall, according to the TPRs among four types of models, the best performance was obtained by using Temporal feature with SVM classifier, which was in accord with the 6-class classification results shown in Fig. 6.

TABLE II shows the subject-independent peak accuracies and peak times. For the peak accuracy, the two-factor repeated measure ANOVA found that there were significant difference between classification features ($F(1,28) = 13.74$, $p = 0.0009$), and no significant difference between classifiers ($F(1,28) = 2.53$, $p = 0.1226$). Furthermore, no significant interaction was found between classification feature and classifier ($F(1,28) = 0.08$, $p = 0.7812$). For the peak time, the two-factor repeated measure ANOVA found that there were no significant difference between classification features ($F(1,28) = 0.02$, $p = 0.8958$), and no significant difference between classifiers

($F(1,28) = 0.16$, $p = 0.6948$). Furthermore, no significant interaction was found between classification feature and classifier ($F(1,28) = 0.02$, $p = 0.8958$). The best decoding performance was obtained by using Temporal feature and SVM

TABLE III. ONE-VERSUS-ONE BINATY CLASSIFICATION ACCURACIES BY USING TEMPORAL AND SPECTRAL FEATURES WITH LDA AND SVM CLASSIFIERS. THE RESULTS WERE AVERAGED ACROSS ALL SUBJECTS.

LDA	Left	Right	Left-Up	Right-Up	Left-Down	Right-Down
Left		0.7851	0.8430	0.8706	0.8149	0.8570
Right	0.7323		0.8580	0.9098	0.8683	0.8691
Left-Up	0.7662	0.8401		0.8680	0.8327	0.8787
Right-Up	0.7652	0.7727	0.7982		0.9031	0.9102
Left-Down	0.7269	0.7666	0.7558	0.7909		0.8312
Right-Down	0.7728	0.7496	0.8201	0.7510	0.7755	

Temporal (green) — Spectral (purple)

SVM	Left	Right	Left-Up	Right-Up	Left-Down	Right-Down
Left		0.8272	0.8531	0.8953	0.8394	0.8734
Right	0.7628		0.8916	0.9172	0.8675	0.8653
Left-Up	0.7972	0.8353		0.9028	0.8566	0.9000
Right-Up	0.8075	0.7947	0.8356		0.9253	0.9044
Left-Down	0.7703	0.7822	0.7947	0.8325		0.8778
Right-Down	0.8175	0.7959	0.8350	0.7731	0.8150	

Temporal (orange) — Spectral (blue)

classifier, with the average peak accuracy of 70.29%± 10.85%.

D. Binary Classification Performance

TABLE III presents the one-versus-one binary classification results by using Temporal and Spectral features with LDA classifier and SVM classifier, respectively. With 6 kinds of movement conditions, 15 binary combinations were yielded. The decoding accuracies were calculated on the window [0.5 1.5] s, because the average peak time calculated by four types of models was 1.01 s (as shown in TABLE II). From TABLE III, we can see that slightly worse classification results were similarly obtained by left-and-right classification combinations in four types of models. This result was in accord with the TPRs shown in TABLE I, which showed the TPRs under the movement condition of left was lower than other movement conditions, and the predicted labels were mainly mistaken for the movement condition of right. By comparing the binary classification results between using Temporal feature and Spectral feature, better classification results were obtained by using Temporal feature with 5% to 10% higher than using Spectral feature for each binary classifier. This conclusion was also in accord with the results shown in Fig. 6 and TABLE II.

IV. DISCUSSION

In this paper, we investigated the neural signatures and decoding of the hand movement direction under conditions of single-hand movement and both-hand movement by using EEG signals. Neural signatures were represented in the forms of the MRCPs at electrodes C1, Cz and C2. The decoding models by using Temporal and Spectral features with LDA and SVM classifiers were built. This paper is the first work to investigate the neural signatures and decoding of hand movement parameters under single-hand and both-hand movement conditions.

We found that different negative offset amplitudes were obtained under six types of movement conditions (as shown in Fig. 3). Different negative offset amplitudes might be in favor of the 6-class movement directions classification. Furthermore, larger negative offset amplitudes were observed under the condition of both-hand movement than under the condition of single-hand movement. This result was consistent with the findings in [15]. Similar results were observed under the condition of left-hand movement in the *up* direction than in the *down* direction, and were also observed under the condition of right-hand movement in the *left* direction than in the *right* direction. These results may be explained according to the findings in [27]. It showed that the negative offset maximum of MRCP might be related to the torque-level, and the negative offset maximum of MRCP in the task with the high torque was higher than that in the same task with the low torque. In our experiment, the torque-level for the both-hand movement was higher than that for the single-hand movement. Furthermore, according to the findings in [28], the torque-level for the movement away from the torso (i.e., the left-hand movement in the *up* direction in our study) was higher than that for the movement toward the torso (i.e., the left-hand movement in the *down* direction in our study), and also the torque-level for the right arm with the leftward motion was higher than that for the right arm with the rightward motion. Besides, for the single-hand (right hand) movement, the lateralization effect was observed with a larger negative offset amplitude of MRCP at electrode C1 than at electrode C2 (as shown in Fig. 4). For the both-hand movement, no lateralization effect was observed.

Experimental results showed that, for 6-class movement directions decoding, the decoding model built by using the Temporal feature and SVM classifier reached the grand average peak accuracy at 70.29%. The differences of negative offset amplitudes in MRCPs between different movement conditions could be indicative of the good decoding performance.

Furthermore, as mentioned in [29], EEG signals are nonlinear and unsteady. From this aspect, the models built by using SVM classifier outperforming those built by using LDA classifier might be because the former can better capture the nonlinear information.

As shown in Fig. 6, the decoding performance higher than chance level (16.67%) was observed both in the movement preparation period (-2 s to 0 s) and in the movement execution period (0 s to 2 s). The decoding performance kept steady during the movement preparation period and gradually increased and peaked during the movement execution period. Since, in our experiment, the movement direction cue was presented at -4 s, the motion intention was already involved in EEG signals during the movement preparation period (-2 s to 0 s), which could lead to higher decoding accuracy than chance level during the preparation period. Besides, after 0 s, the actual movement started to be executed. With the shifted windows, more neural information related to hand motor was gradually involved in the decoding window, leading to the increment of decoding performance.

Compared to the latest studies [15] on unimanual and bimanual actions decoding, we could obtain a better decoding result. The grand average participant-specific peak accuracy reached 38.6% at 1.11s for 7-class classification in [15], and reached 70.29% at 1.00 s for 6-class classification in our study. However, one should note that since the movement parameter to be decoded (movement type in [15], and movement direction in our study), EEG amplifier, and subjects were different between the mentioned work and our work, the direct comparison in decoding accuracy is unfair.

This work has vital values in the following implications. The cooperation of both hands was common, such as one hand to operate steering wheel and the other hand to operate gear lever in the human-vehicle interaction system. From this aspect, the discrimination of single-hand movement from both-hand movement should be explored. Furthermore, though the discrimination of unimanual and bimanual reach-and-grasp actions has been studied in [15], the primary purpose of their study was for bimanual neuroprostheses. The tasks in daily life were abstracted to decode different types of actions, such as holding the spoon and jar. However, in practice, for most human-machine interaction systems, decoding the hand movement parameters (such as direction and velocity) of operators is more useful. Thus, this work can lay a foundation for the future development of an active human-machine collaboration system based on EEG signals and open a new research direction in the field of decoding hand movement parameters from EEG signals.

However, there are still some limits in this work, which need to be addressed in our future work. First, although the relatively good averaged performance was obtained by using the Temporal feature and SVM classifier, subject differences in decoding performance were observed. As presented in TABLE II, when using the Temporal-SVM model, relatively low peak accuracies were obtained for Subjects 2, 4, 5, and 8. One possible method to address the problem is to build the subject-specific models by using different features and classifiers [30] [31]. Second, in our study, we focused on the movement direction decoding from EEG signals. To better apply both-

hand movement decoding-based BCIs to human-machine interaction systems, more types of movement kinematics parameters should be decoded, such as velocity, acceleration, trajectory construction, and also more kinds of information should be fused to improve the stability and scalability of systems, e.g., the priori-knowledge of hand movement given a specified task, machine states, and environment information. Third, in this work, we analyzed the discrimination of the single-hand movement from both-hand movement in an offline way. To apply the proposed method to develop brain-controlled assistive devices, we should design a corresponding brain-machine interface and test it online. Finally, in our experiment, to explore the feasibility of decoding single-hand and both-hand movement directions, we assumed the right-hand movement in horizontal directions (right or left). Considering that, in human-machine collaboration systems, two hands often move in different directions, we preliminarily set the left-hand movement in vertical directions (up or down) rather than horizontal directions. In other words, we took the four-class both-hand movements and two-class single-hand movements as an example to explore the feasibility to decode single-hand and both-hand movement directions. It is a challenge to differentiate multiple types of movements from EEG signals. This work tries to extend the hand movement decoding to 6 classes to prove the concept. We will study more classes in the future.

Our future work will be focused on addressing these limits mentioned above, including improving decoding performance, decoding more types of movement parameters and more combinations of movement directions, using more subjects, and conducting the online test.

V. CONCLUSION

Our study shows the feasibility of discriminating single-hand and both-hand movement directions by using the low-frequency EEG signals. Neural signatures were presented in the form of MRCPs. Larger negative offset amplitudes were observed under the condition of both-hand movements. By using EEG potentials as features with the SVM classifier, peak decoding accuracy was obtained at 70.29% for six-class classification. This work first explores the decoding of single-hand and both-hand movement directions and can contribute to developing an active human-machine collaboration system.

ACKNOWLEGEMENT

REFERENCES

[1] C. K. Cui *et al.*, "A Multimodal Framework Based on Integration of Cortical and Muscular Activities for Decoding Human Intentions About Lower Limb Motions," *IEEE Transactions on Biomedical Circuits and Systems*, vol. 11, no. 4, pp. 889-899, Aug, 2017.

[2] R. Leeb *et al.*, "A hybrid brain-computer interface based on the fusion of electroencephalographic and electromyographic activities," *Journal of Neural Engineering*, vol. 8, no. 2, Apr, 2011.

[3] S. Haufe *et al.*, "EEG potentials predict upcoming emergency brakings during simulated driving," *Journal of Neural Engineering*, vol. 8, no. 5, Oct, 2011.

[4] T. Teng *et al.*, "EEG-Based Detection of Driver Emergency Braking Intention for Brain-Controlled Vehicles," *IEEE Transactions on*

Intelligent Transportation Systems, vol. 19, no. 6, pp. 1766-1773, Jun, 2018.

[5]   L. A. Farwell, and E. Donchin, "Talking off the top of your head: toward a mental prosthesis utilizing event-related brain potentials," *Electroencephalography and Clinical Neurophysiology*, vol. 70, no. 6, pp. 510-523, Dec, 1988.

[6]   J. R. Wolpaw *et al.*, "An EEG-based brain-computer interface for cursor control," *Electroencephalography and Clinical Neurophysiology*, vol. 78, no. 3, pp. 252-259, Mar, 1991.

[7]   L. Bi *et al.*, "Using a Head-up Display-Based Steady-State Visually Evoked Potential Brain-Computer Interface to Control a Simulated Vehicle," *IEEE Transactions on Intelligent Transportation Systems*, vol. 15, no. 3, pp. 959-966, Jun, 2014.

[8]   B. J. Edelman *et al.*, "Noninvasive neuroimaging enhances continuous neural tracking for robotic device control," *Science Robotics*, vol. 4, no. 31, Jun 19, 2019.

[9]   P. Ofner *et al.*, "Attempted Arm and Hand Movements can be Decoded from Low-Frequency EEG from Persons with Spinal Cord Injury," *Scientific Reports*, vol. 9, May 9, 2019.

[10]   S. Waldert *et al.*, "Hand movement direction decoded from MEG and EEG," *Journal of Neuroscience*, vol. 28, no. 4, pp. 1000-1008, Jan 23, 2008.

[11]   T. J. Bradberry *et al.*, "Decoding three-dimensional hand kinematics from electroencephalographic signals," *2009 Annual International Conference of the IEEE Engineering in Medicine and Biology Society,* Vols. 1-20, pp. 5010-, 2009.

[12]   N. Robinson *et al.*, "Multi-class EEG classification of voluntary hand movement directions," *Journal of Neural Engineering*, vol. 10, no. 5, Oct, 2013.

[13]   M. Jochumsen *et al.*, "Detecting and classifying movement-related cortical potentials associated with hand movements in healthy subjects and stroke patients from single-electrode, single trial EEG," *Journal of Neural Engineering*, vol. 12, no. 5, Oct, 2015.

[14]   T. Chouhan *et al.*, "Wavlet phase-locking based binary classification of hand movement directions from EEG," *Journal of Neural Engineering*, vol. 15, no. 6, Dec, 2018.

[15]   A. Schwarz *et al.*, "Unimanual and bimanual reach-and-grasp actions can be decoded from human EEG," *IEEE Transactions on Biomedical Engineering*, 2019.

[16]   N. Robinson *et al.*, "EEG-Based Classification of Fast and Slow Hand Movements Using Wavelet-CSP Algorithm," *IEEE Transactions on Biomedical Engineering*, vol. 60, no. 8, pp. 2123-2132, Aug, 2013.

[17]   C. Toro *et al.*, "Event-Related desynchronization and movement-related cortical potentials on the ECOG and EEG," *Electroencephalography and Clinical Neurophysiology*, vol. 93, no. 5, pp. 380-389, Oct, 1994.

[18]   F. Karimi *et al.*, "Detection of movement related cortical potentials from EEG using constrained ICA for brain-computer interface applications," *Frontiers in Neuroscience*, vol. 11, Jun 30, 2017.

[19]   D. Liu *et al.*, "EEG-Based lower-limb movement onset decoding: continuous classification and asynchronous detection," *IEEE Transactions on Neural Systems and Rehabilitation Engineering*, vol. 26, no. 8, pp. 1626-1635, Aug, 2018.

[20]   C.-Y. Chang *et al.*, "Evaluation of Artifact Subspace Reconstruction for Automatic Artifact Components Removal in Multi-Channel EEG Recordings," *IEEE Transactions on Biomedical Engineering*, vol. 67, no. 4, pp. 1114-1121, Apr, 2020.

[21]   A. T. Tzallas *et al.*, "Epileptic seizure detection in EEGs using time-frequency analysis," *IEEE Transactions on Information Technology in Biomedicine*, vol. 13, no. 5, pp. 703-710, Sep, 2009.

[22]   T. Teng and L. Bi, "A novel EEG-based detection method of emergency situations for assistive vehicles", *2017 Seventh International Conference on Information Science and Technology (ICIST)*, 16-19 April 2017, IEEE, Piscataway, NJ, USA, 2017, pp. 335-9.

[23]   A. Subasi and M. I. Gursoy, "EEG signal classification using PCA, ICA, LDA and support vector machines," *Expert Systems with Applications*, vol. 37, no. 12, pp. 8659-8666, Dec, 2010.

[24]   C. C. Chang and C. J. Lin, "LIBSVM: A library for support vector machines," *ACM Transactions on Intelligent Systems and Technology*, vol. 2, no. 3, 2011.

[25]   L. Bi *et al.*, "Effects of symmetry and number of compositional elements on Chinese users' Aesthetic Ratings of Interfaces: Experimental and Modeling Investigations," *International Journal of Human-Computer Interaction*, vol. 27, no. 3, pp. 245-259, 2011.

[26]   Z. Khaliliardali *et al.*, "Action prediction based on anticipatory brain potentials during simulated driving," *Journal of Neural Engineering*, vol. 12, no. 6, Dec, 2015.

[27]   Y. Gu *et al.*, "Identification of task parameters from movement-related cortical potentials," *Medical & Biological Engineering & Computing*, vol. 47, no. 12, pp. 1257-1264, Dec, 2009.

[28]   S. S. Chan, and D. W. Moran, "Computational model of a primate arm: from hand position to joint angles, joint torques and muscle forces," *Journal of Neural Engineering*, vol. 3, no. 4, pp. 327-337, Dec, 2006.

[29]   T. Ning and J. D. Bronzino, "Nonlinear Analysis of the Hippocampal Subfields of CAl and the Dentate Gyrus," *IEEE Transactions on Biomedical Engineering*, vol. 40, no. 9, Sep, 1993.

[30]   B. Blankertz *et al.*, "The non-invasive Berlin Brain-Computer Interface: Fast acquisition of effective performance in untrained subjects," *Neuroimage*, vol. 37, no. 2, pp. 539-550, Aug 15, 2007.

[31]   J.-H. Jeong *et al.*, "Decoding Movement-Related Cortical Potentials Based on Subject-Dependent and Section-Wise Spectral Filtering," *IEEE Transactions on Neural Systems and Rehabilitation Engineering*, vol. 28, no. 3, pp. 687-698, Mar, 2020.